

THE CANADIAN MINERALOGIST

Journal of the Mineralogical Association of Canada

Volume 20

February 1982

Part 1

Canadian Mineralogist
Vol. 20, pp. 1-18 (1982)

STRUCTURAL ASPECTS OF GREENALITE AND RELATED MINERALS

STEPHEN GUGGENHEIM

*Department of Geological Sciences, University of Illinois at Chicago,
Chicago, Illinois 60680, U.S.A.*

S.W. BAILEY

*Department of Geology and Geophysics, University of Wisconsin-Madison,
Madison, Wisconsin, 53706, U.S.A.*

R.A. EGGLETON

*Department of Geology, Australian National University,
Canberra, A.C.T. 2600, Australia*

PETER WILKES

*Department of Metallurgical and Mineral Engineering,
University of Wisconsin-Madison, Madison, Wisconsin 53706, U.S.A.*

ABSTRACT

Both a trigonal and a monoclinic phase are present in all studied samples of greenalite and of its Mn-analogue, caryopilite. Whenever the relative orientations could be determined, the two phases were found to be in a fixed, coherent intergrowth with one phase either rotated by 180° (or $\pm 60^\circ$) relative to the other or inverted without rotation. On $hk0$ electron-diffraction photographs, the $k = 3n$ reflections are sharp and are surrounded by incomplete hexagons of satellites directed along the three pseudo-hexagonal Y^* axes. The satellite spacings indicate a regular but irrational modulation of the conventional structure of the subcell, which varies from $23 \text{ \AA} = 2.4b$, in greenalite to $17 \text{ \AA} = 1.7b$, in caryopilite. The $k \neq 3n$ reflections have zero intensity at the lattice points. Outside these lattice points there is a distribution of diffuse intensity that varies from two to three ill-defined blobs to three sharper satellite or superlattice spots. Dark field and bright field electron micrographs from the $hk0$ patterns show three sets of intersecting fringes normal to the three pseudo-hexagonal Y^* axes, which can be resolved into domains consisting of a small number of six-member rings. The domain boundaries are poorly resolved, and there is considerable defect nature in the size, shape and lateral disposition of the domains. Fringes seen normal to the layers

have a crinkled to sinusoidal appearance in places. A model supported by optical simulation is proposed for greenalite consisting of saucer-shaped island domains four tetrahedral rings in diameter. One extra tetrahedron is inserted into the tetrahedral sheet every eight tetrahedra to create antiphase relations between adjacent tetrahedral islands and to facilitate articulation with the larger octahedral sheet. Four-member and three-member rings joining adjacent islands may be inverted and coordinate with the octahedral sheet of the adjacent layer. The satellites around $k = 3n$ reflections are believed due to a regular doming of the octahedral portions of the saucers and to the omission of rows of octahedral cations around the island edges. Tetrahedral islands coordinate randomly with anions of the octahedral sheet in greenalite, but more regularly in at least one sample of caryopilite having sharper $k \neq 3n$ satellites. The islands in caryopilite are three rings in diameter. The relation of the intergrown trigonal and monoclinic phases to the island domains is not known.

Keywords: greenalite, caryopilite, serpentine, minnesotaite, X-ray, TEM, HRTEM.

SOMMAIRE

Tous les échantillons de greenalite et de caryopilite, son analogue manganifère, contiennent une

phase trigonale et une autre monoclinique, Dans chacun des cas où leurs orientations relatives ont pu être vérifiées, les deux phases montrent la même intercroissance cohérente, l'une des phases étant soit tournée de 180° (ou $\pm 60^\circ$) par rapport à l'autre, soit inversée sans rotation. Sur des clichés de diffraction électronique, les réflexions $k = 3n$ du plan $hk0$ sont nettes et entourées d'hexagones incomplets de satellites dirigés le long des trois axes pseudo-hexagonaux Y^* . L'espacement de ces satellites indique une modulation régulière mais irrationnelle de la structure conventionnelle de la sous-maille, qui varie de 23 \AA ($= 2.4b_c$) dans la greenalite à 17 \AA ($= 1.7b_c$) dans la caryopillite. Les réflexions $k \neq 3n$ ont une intensité nulle aux noeuds du réseau. Entre les noeuds, on observe une distribution diffuse d'intensité allant de deux ou trois taches mal définies à trois réflexions satellites ou de surstructure nettes. Les photomicrographies électroniques sur fond obscur et sur fond clair, dérivées des clichés $hk0$, montrent trois systèmes de franges concourants, perpendiculaires aux trois axes pseudo-hexagonaux Y^* ; on peut résoudre ceux-ci en domaines aux limites imparfaitement définies qui contiennent un petit nombre d'anneaux à six membres. La dimension, la forme et la disposition latérale des domaines sont irrégulières. Par endroits, les franges perpendiculaires aux feuillettes ont une apparence ondulée à sinusoïdale. Selon un modèle étayé par simulation optique, la greenalite serait formée d'îlots en forme de soucoupe ayant un diamètre de quatre anneaux de tétraèdres. Un tétraèdre supplémentaire est inséré dans le feuillet tétraédrique tous les huit tétraèdres. Les îlots adjacents sont ainsi en relation d'antiphase, ce qui facilite l'articulation avec le feuillet octaédrique plus grand. Les anneaux à quatre et à trois membres qui lient les îlots adjacents peuvent être inversés pour permettre la liaison avec les couches octaédriques des feuillettes adjacents. Les satellites autour des réflexions $k = 3n$ seraient dus à un bombement régulier des portions octaédriques des soucoupes et à l'omission de rangées de cations octaédriques en bordure des îlots. Ces îlots de tétraèdres sont coordonnés de façon aléatoire aux anions de la couche octaédrique dans la greenalite, mais plus régulièrement dans au moins un exemple de caryopillite qui possède des réflexions satellites $k \neq 3n$ plus nettes. Dans la caryopillite, le diamètre des îlots équivaut à trois anneaux. La relation entre l'intercroissance des phases trigonale et monoclinique et les domaines insulaires reste à déterminer.

(Traduit par la Rédaction)

Mots-clés: greenalite, caryopillite, serpentine, minnesotaïte, rayons X, microscopie électronique à transmission, microscopie électronique à transmission de haute résolution.

INTRODUCTION

The crystal structures of hydrous phyllosil-

icate minerals are based on layers that contain tetrahedrally and octahedrally coordinated sheets in either 1:1 or 2:1 ratios. Adjacent layers, which may be separated from one another by various interlayer materials, often can be superimposed in different geometric patterns to create polytypes with different symmetries and periodicities normal to the layers. For example, the serpentines based on planar 1:1 layers have been identified by X-ray techniques as having one-layer trigonal (1*T*), two-layer hexagonal (2*H*) and six-layer trigonal (6*T*) structures; a similar diversity is observed in many other 1:1 and 2:1 layer species.

The degree of fit between the lateral dimensions of the component tetrahedral and octahedral sheets, which must have common planes of junction within a layer, has a profound influence on the resultant crystal size, morphology and structure of the mineral (Roy & Roy 1954, Bates 1959). In the majority of layer silicates, the ideal lateral dimensions of the tetrahedral sheet are larger than those of the octahedral sheet. Zviagin (1957) and Radoslovich (1961) have shown that it is relatively easy to reduce the lateral dimensions of a tetrahedral sheet by rotating adjacent tetrahedra in opposite directions in the (001) plane. It is more difficult to stretch the lateral dimensions of a tetrahedral sheet to fit those of a larger octahedral sheet; consequently, the structural adjustment may be more drastic. Mechanisms observed to date in layer silicates include adjustment of sheet thicknesses, with corresponding changes in lateral dimensions, in sudoite (Eggleton & Bailey 1967), buckling of the octahedral cation plane in lizardite (Krstanović 1968), tetrahedral tilting leading to continuous curling in the case of the 1:1 layers of chrysotile (Jagodzinski & Kunze 1954), inversion and relinkage of tetrahedral apical directions in a periodic pattern in stilpnomelane (Eggleton 1972) and tetrahedral tilting plus inversion in antigorite (Zussman 1954, Kunze 1956). Examples requiring these latter mechanisms are restricted to phyllosilicate species with little or no tetrahedral substitution for Si and with octahedral sheets populated with divalent cations of the size of Mg, Ni, Fe, Mn and Co.

Cylindrical rolls of 1:1 layers, with the larger octahedral sheet on the convex side and the smaller tetrahedral sheet on the concave side, are the rule for the chrysotile serpentines of composition $\text{Mg}_3\text{Si}_2\text{O}_5(\text{OH})_4$ (Bates *et al.* 1950). Ni^{2+} ($r = 0.69 \text{ \AA}$) is similar in size to Mg^{2+} ($r = 0.72 \text{ \AA}$) in octahedral coordination (Shannon 1976); similar asbestiform fibres are observed for pecoraite, the Ni analogue of

clinochrysotile (Faust *et al.* 1969), and for some garnieritic ores of Ni (Uyeda *et al.* 1973). Fibrous Mg- and Ni-chrysotiles have been synthesized (Noll & Kirchner 1952, Roy & Roy 1954), as have the Co^{2+} - and Fe^{2+} -analogues ($r = 0.745$ and 0.78 \AA , respectively; Noll *et al.* 1958, Jasmund & Sylla 1970), but the latter two have not been recognized in nature to date. Octahedral sheets rich in Fe^{2+} and Mn^{2+} ($r = 0.83 \text{ \AA}$) provide an especially poor fit with the lateral dimensions of a Si-rich tetrahedral sheet, so that some type of major structural accommodation must take place. Greenalite and caryopillite have 1:1 layers with compositions of this type, but electron micrographs show no evidence of chrysotile-like fibres. Minnesotaitite also is Fe^{2+} -rich, but its $d(001)$ value of 9.6 \AA suggests a 2:1 layer (Gruner 1944). The tendency for curling in such a layer would be canceled by sandwiching the misfit octahedral sheet between two tetrahedral sheets. Some method of structural compensation other than curling can be anticipated in greenalite, caryopillite and minnesotaitite.

Greenalite and minnesotaitite are hydrous iron-rich phyllosilicates that commonly occur in low-grade metamorphic iron-formations (Leith 1903, Gruner 1944). Because both minerals typically occur as fine grained particles intermixed with other minerals, early studies were primarily of a qualitative nature, involving X-ray powder photographs of mixtures of mineral phases and comparison of approximate chemical compositions. Although limited by such data, Gruner (1936, 1944) suggested that greenalite and minnesotaitite were the ferrous iron analogues of serpentine and talc, respectively. Steadman & Youell (1958) determined the cell dimensions of a single greenalite sample, and suggested that it is most similar to the platy serpentine now known as berthierine but called chamosite in much of the older literature.

Floran & Papike (1975) have determined from electron-microprobe analyses that the compositions of greenalite and minnesotaitite deviate from those expected for the ferrous analogues of serpentine and talc. They attributed an observed Si excess and total octahedral deficiency in greenalite as due either to a mechanical mixture with small amounts of minnesotaitite or, more likely, to a periodic alternating-wave structure transitional between platy serpentine and minnesotaitite. They predicted tetrahedral inversion in greenalite due to tetrahedral-octahedral misfit, similar to the inversion in antigorite but differing from the latter in requiring the formation of small 2:1 layer regions of minnesotaitite at the inversion

loci of the waves. Minnesotaitite, on the other hand, was found to have a small deficiency of Si and a corresponding excess of total octahedral cations. Floran & Papike (1975) suggested that these deviations from the ideal minnesotaitite formula may be due to tetrahedral inversions that create small greenalite-like regions in the structure.

GREENALITE

Electron-microprobe results

In the present study several samples with small areas of pure greenalite were found, with the result that the compositions and X-ray powder patterns could be determined unambiguously. The samples studied are listed in Table 1.

In most cases, the electron-microprobe results were determined on the same solid grains for which X-ray powder patterns had been obtained previously. Probe analyses were obtained on two different instruments by five different operators, and the results were then compared and collated. The agreement was good; the results in Table 2 are in most cases the average of 10 to 16 individual analyses.

TABLE 1. GREENALITE SAMPLES STUDIED

Locality and Occurrence	Donor
1. Biwabik iron formation, Cincinnati mine near Biwabik, Minn., U.S.A. Huronian age granules in chert. Leith type specimens #45765 and 45766.	S. A. Tyler
2. Biwabik iron formation, Minn., U.S.A. Huronian age granules in chert. Leith coll. #223	S. A. Tyler
3. Bluebell Pb-Zn mine, Riondel, British Columbia, Canada. Tertiary hydrothermal replacement of Cambrian limestone in fracture zones.	L. Moyd
4. San Valentin Pb-Zn-Fe open pit mine in Cartagena mining district, La Union, Murcia, Spain. Subvolcanic-hydrothermal late Tertiary replacement of limestone.	A. Arribas
5. Arenig outcrop near Glenluce, Wigtownshire, Scotland, in Ordovician ferruginous cherts associated with spilitic pillow lavas. Inst. Geol. Sci. spec. #ED70.	B. Young
6. Gunflint iron formation NE of Gunflint Lake, Ontario, Canada. Huronian age granules in Upper Gunflint taconite. Goodwin spec. #108-51.	A. M. Goodwin
7. Gunflint iron formation. Cryptocrystalline and coarse-grained acicular granules. Spec. #724-1A of Floran & Papike (1975).	R. J. Floran
8. Sokoman iron formation at Knob Lake, Labrador, Canada. Proterozoic age granules in chert. Spec. #Z-91 of Zajac (1974).	I. S. Zajac

TABLE 2. ELECTRON PROBE ANALYSES OF GREENALITE

	Bwabik I.F., Leith #45765				Bluebell mine, Rondel, B.C.				Sierra de Cartagena, Spain			
	1	2	3	4	1	2	3	4	1	2	3	4
Si	34.7%	2.057	1.941	2.000	36.5%	2.129	1.984	2.000	35.9%	2.099	1.990	2.000
Al	0.90	.063	.059	.061	0.25	.017	.016	.016	0.16	.011	.010	.010
Fe*	47.3	2.344	2.212	2.279	40.2	1.961	1.828	1.842	47.8	2.337	2.216	2.227
Mn	0.15	.007	.007	.007	8.71	.431	.401	.404	1.78	.088	.084	.084
Mg	4.98	.440	.415	.428	3.75	.326	.304	.305	4.13	.360	.341	.343
□		.146	.366	.225		.265	.467	.432		.204	.359	.336
Na	0.00				n.d.				n.d.			
K	0.00				n.d.				n.d.			
Ca	0.00				n.d.				n.d.			
Σ	88.03				89.41				89.77			

	Arenig, Scotland, #ED70				Gunflint I.F., #724-1A				Sokoman I.F., Zajac #Z-91			
	1	2	3	4	1	2	3	4	1	2	3	4
Si	34.4%	2.079	1.997	2.000	35.9%	2.103	1.996	2.000	36.5%	2.123	1.990	2.000
Al	0.05	.004	.003	.003	0.06	.004	.004	.004	0.16	.011	.010	.010
Fe*	55.5	2.805	2.694	2.698	50.0	2.450	2.325	2.330	46.7	2.272	2.129	2.140
Mn	0.18	.009	.009	.009	0.06	.003	.003	.003	1.50	.074	.069	.069
Mg	0.26	.023	.022	.022	3.83	.334	.317	.318	4.53	.393	.368	.370
□		.159	.275	.268		.209	.355	.345		.250	.434	.411
Na	0.08				n.d.				n.d.			
K	0.00				0.00				n.d.			
Ca	0.00				0.00				0.02			
Σ	90.47				89.85				89.41			

	Gunflint I.F., Goodwin #108-51					* All Fe reported as FeO
	1	2	3	4	5	
Si	36.3%	2.106	1.993	2.000	2.035	1 Weight percentage of oxides
Al	0.10	.007	.007	.007	.007	2 Atoms on basis of 7.0 oxygens
Fe ²⁺	50.4	2.446	2.315	2.322	1.891	3 Atoms on basis of 2.0 Si+Al tetrahedral cations
Fe ³⁺					.473	4 Atoms on basis of 2.0 Si tetrahedral cations
Mn	0.06	.003	.003	.003	.003	5 Atoms on basis of 7.0 oxygens and for Fe ²⁺ /Fe ³⁺ ratio determined by Mössbauer analysis
Mg	3.80	.328	.311	.312	.317	
□		.216	.371	.356	.309	
Na	0.17					
K	0.04					
Ca	0.00					
Σ	90.87					

Individual analyses were discarded only if there was tangible evidence of impurity phases or of water volatilization. One set of analyses was done on the University of Wisconsin ARL microprobe, using wavelength dispersion and the correction procedure of Bence & Albee (1968), with incorporation of the alpha factors of Albee & Ray (1970). The second set of analyses was done on the University of Chicago ARL microprobe, using energy dispersion and similar correction procedures. In all cases the electron beam was broadened and the sample current kept as low as possible in order to minimize volatilization of water.

The electron-microprobe analyses confirm the microprobe analyses of Floran & Papike (1975), and show a consistent Si excess and octahedral deficiency for greenalite based on the assumption of 7 oxygens in a serpentine-like structure. Points to note about these analytical results are the virtual absence of Al_2O_3 and the presence of 3-4% MgO and of some MnO in most samples. In the Bluebell mine sample, ~9% MnO proxies for FeO. The apparent Si excess ranges from 0.06 to 0.13 atoms per formula unit for the seven analyses. The apparent octahedral deficiency ranges from 0.15 to 0.27 atoms. A

Mössbauer analysis of a Gunflint sample by Wayne A. Dollase of UCLA (pers. comm. 1973) gave a $Fe^{2+}:Fe^{3+}$ ratio of 79.8:20.2. Because of the tetrahedral Si excess, all of the Fe^{3+} is considered to be in octahedral coordination in this structure. The effect of the Fe^{3+} is to reduce the apparent Si excess and to increase the apparent octahedral deficiency. None of the other greenalite specimens could be purified sufficiently for Mössbauer analysis.

X-ray study

Because greenalite is already fine grained in its natural state, no grinding was necessary to obtain X-ray powder lines of uniform density. Impurities were minimized by careful microscopic selection from the bulk samples of millimetre-sized greenalite granules, which were glued onto the tips of glass fibres for individual X-ray study. It proved to be possible in this manner to obtain at least a few patterns completely free of other phyllosilicates, including minnesotaite, in all of our samples and free of quartz in most samples. In indexing the patterns we have assumed orthohexagonal lattices for reasons of convenience and accuracy. Although

a metrically trigonal phase is dominant in greenalite, it is doubtful whether the true symmetry of this phase is trigonal.

X-ray powder patterns of pure greenalite samples show the presence of two Fe-rich serpentine phases that have the $00l$ and $06l$ reflections in common. Of the nonoverlapping reflections, the most intense can be indexed as $20l$ and $40l$ reflections of a group-C structure as derived by Bailey (1969) and in approximate agreement with the cell dimensions of Steadman & Youell (1958). The three possible group-C structures ($1T$, $2T$ and $3R$) are characterized by occupation of the same set of octahedral positions (I or II) in every layer and by interlayer shifts of zero or $b/3$. The calculated $h0l$ reflections for these three structures are identical in spacing and intensity, and none of the weak $k \neq 3n$ reflections that are diagnostic in distinguishing between the three structures is present on the photographs. An equal number of additional but weaker reflections are present that give a good fit with the d values and

intensities calculated for $h0l$ reflections for an iron-rich serpentine belonging to the group-A polytypes of Bailey (1969). The three ideal group-A polytypes ($1M$, $2M_1$ and $3T$) are characterized by the occupation of the same set of octahedral positions in every layer and by interlayer shifts of $a/3$ along one, two or three of the pseudohexagonal X axes, respectively. The calculated $h0l$ reflections are identical in spacing and intensity for these three structures also, although different from those of the group-C structures, and diagnostic $k \neq 3n$ reflections are not present. For the Bluebell mine specimen, the extra group-A reflections are much more intense than in the other six samples (e.g., pattern B relative to pattern A in Fig. 1). According to intensity calculations, the monoclinic group-A phase is only slightly less abundant than the trigonal group-C phase in this specimen.

One small, imperfect crystal was located in the Bluebell mine sample. A Gandolfi powder pattern of the crystal is identical to that of the

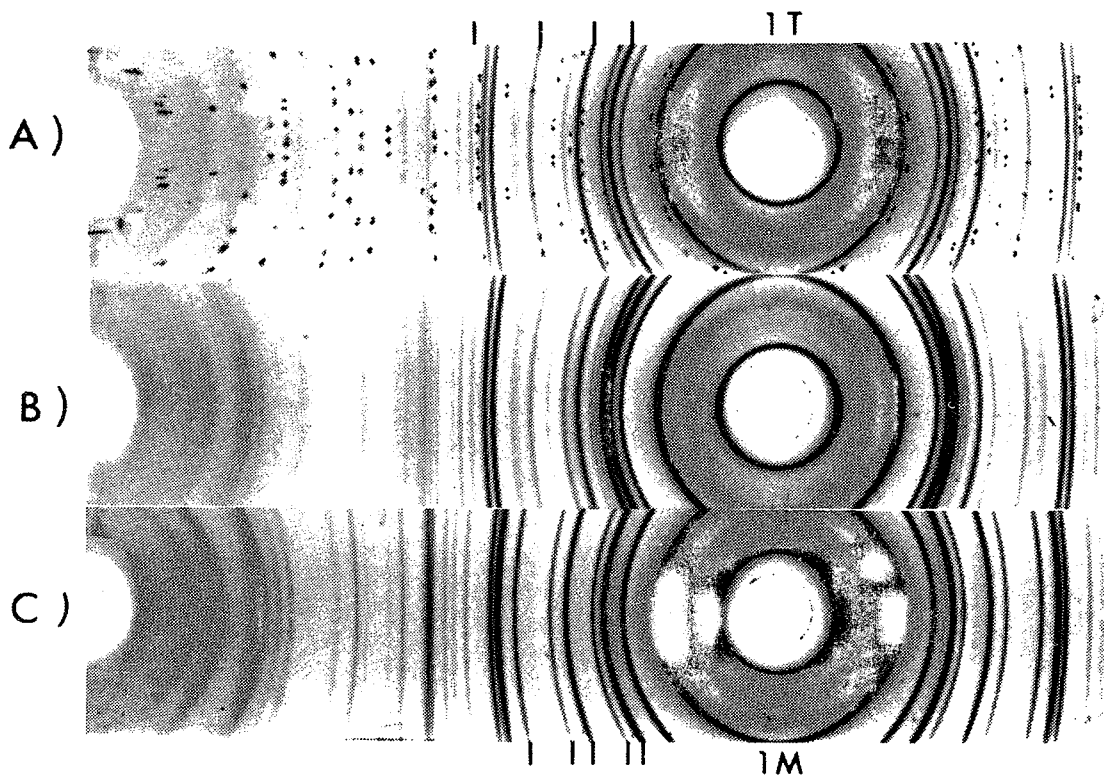


FIG. 1. X-ray powder patterns with monochromatic Fe X-radiation. a) Greenalite from the Gunflint Iron Formation (108-51) with the trigonal phase dominant. Spots are due to coarse quartz particles. b) Greenalite from the Bluebell mine with the trigonal and monoclinic phases about equally abundant. c) Caryopilite from the Olympic Peninsula (S-60-14-16) with the monoclinic phase dominant.

fine grained greenalite from the same sample and shows that the crystal also is an intergrowth of two phases. Although not suitable for detailed structural analysis, the crystal proved sufficiently well organized to allow determination of the nature of the intergrowth. For the group-C phase the 20l reflections are observed, on precession photographs, to be unequal in intensity to those of index 20 \bar{l} and in agreement with calculated values, thus allowing the sense (+ or -) of the axes to be determined. The group-A phase is in a fixed orientation relative to the group-C phase. All reflections have mosaic spread, and the diffuse $k \neq 3n$ reflections of the two structures merge in such a way that it is not possible to identify either phase as a specific polytype or even to conclude that the stacking is regular rather than random. The 20l row line contains several reflections from the two structures that do not overlap because of the different β angles. The observed close pairing of the strongest reflection of the group-C structure at $d = 2.605 \text{ \AA}$ on this row line with the strongest group-A reflection at $d = 2.486 \text{ \AA}$ is possible for only two relative orientations of the structures, regardless of the specific polytypes involved.

Either the group-A structure is rotated by 180° (or $\pm 60^\circ$) around Z^* relative to the group-C structure so that the octahedra slant in opposite directions in the two phases, or the group-A layers are inverted relative to the group-C layers but with all octahedra having the same slant. Rotation by 180° or $\pm 60^\circ$ is equivalent to the occupation of a different set of octahedral positions (I versus II) in the two structures.

Although the stacking sequences cannot be determined specifically, even by single-crystal study, they must be different in group-A and group-C structures. The two phases may be called the trigonal (for group C) and monoclinic (for group A) components. They are somewhat similar to the two components in berthierine (Brindley 1951) but differ in that the two phases are in a fixed structural relationship in greenalite but are present as admixtures in berthierine.

The powder pattern of greenalite from the Bluebell mine is shown in Figure 1b, and is listed in Table 3 with the trigonal phase arbitrarily indexed for simplicity as the 1T polytype (but with orthohexagonal indices) and with the monoclinic phase arbitrarily indexed as 1M. It

TABLE 3. X-RAY POWDER PATTERNS OF GREENALITE AND CARYOPILITE

Greenalite (sample 3)						Caryopillite (sample 1)					
1T (calc.)		Observed		1M (calc.)		1T (calc.)		Observed		1M (calc.)	
d(\AA)	hkl	d(\AA)	Int.	d(\AA)	hkl	d(\AA)	hkl	d(\AA)	Int.	d(\AA)	hkl
7.212	001	7.20	100	7.211	001	7.273	001	7.30	80	7.270	001
3.606	002	3.61	50	3.605	002	3.636	002	3.639	50	3.635	002
2.796	200	2.78	30	2.77	20 $\bar{1}$,130			2.825	60	2.822	20 $\bar{1}$,130
2.607	201,131	2.605	60			2.650	201,131	2.648	5		
		2.486	30	2.486	20 $\bar{2}$,131			2.521	100	2.523	20 $\bar{2}$,131
2.404	003	2.408	10	2.404	003	2.424	003	2.427	7	2.423	003
		2.385	10	2.380	201,13 $\bar{2}$			2.382	20	2.384	201,13 $\bar{2}$
2.209	202,132	2.210	40			2.241	202,132	2.239	4		
		2.078	15	2.075	20 $\bar{3}$,132			2.101	35	2.101	20 $\bar{3}$,132
		1.944	5	1.944	202,133			1.968	20	1.969	202,133
1.823	203,133	1.823	15			1.846	203,133	1.850			
		1.715	10	1.712	20 $\bar{4}$,133	1.818	004	1.820	2	1.817	*004
1.614	060,330	1.616	60	1.616	060,331			1.731	25	1.731	20 $\bar{4}$,133
1.575	061,331	1.577	45	1.576	061,330,33 $\bar{2}$	1.643	060,330	1.643	35	1.643	060,331
1.515	204,134	1.519	10					1.626	20	1.627	203,13 $\bar{4}$
1.473	062,332	1.474	15	1.474	062,331,33 $\bar{3}$	1.603	061,331	1.603	25	1.603	061,330,33 $\bar{2}$
1.442	005	1.442	5	1.442	005	1.533	204,134	1.535	3		
1.398	400,260	1.397	10			1.497	062,332	1.497	10	1.497	062,331,33 $\bar{3}$
1.372	401,261	1.373	10			1.455	005	1.455	10	1.454	005
		1.358	5	1.355	400,26 $\bar{2}$			1.420	10	1.445	20 $\bar{5}$,134
1.340	063,333	1.340	10	1.341	063,332,33 $\bar{4}$			1.377	15	1.377	401,26 $\bar{1}$
1.303	402,262	1.302	5					1.367	20	1.366	400,26 $\bar{2}$
1.203	006,064,334	1.202	5	1.202	006,064,333			1.367	20	1.367	204,13 $\bar{5}$
						1.295	205,135	1.295	10	1.294	401,26 $\bar{3}$
								1.260	2	1.261	40 $\bar{4}$,262
						1.219	064,334	1.215	2	1.219	064,333,33 $\bar{5}$
						1.212	006	1.212	006	1.212	006
								1.192	10	1.192	402,26 $\bar{4}$
								1.154	5	1.156	40 $\bar{5}$,263
						1.089	065,335	1.087	10	1.089	065,334,33 $\bar{6}$
										1.085	403,26 $\bar{5}$

a = 5.591 \AA	a = 5.601 \AA
b = 9.685	b = 9.691
c = 7.212	c = 7.453
$\beta = 90^\circ$	$\beta = 104.6^\circ$

a = 5.693 \AA	a = 5.692 \AA
b = 9.854	b = 9.860
c = 7.273	c = 7.513
$\beta = 90^\circ$	$\beta = 104.6^\circ$

Both photographs taken with monochromatized $\text{FeK}\alpha$ radiation in 114.6 mm diameter cameras. Intensities estimated visually. Cell dimensions determined by least-squares fit.

should be noted that the most intense line unique to the monoclinic component at $d = 2.486 \text{ \AA}$ would be overlapped by a quartz impurity line, and that the other unique lines are much weaker. Two of these weaker lines at $d = 2.355$ and 1.358 \AA would be overlapped by siderite impurity lines. This overlap undoubtedly explains why the monoclinic component has not been reported previously. Although the greenalite powder pattern published by Gruner (1936) has been indexed by Bayliss (1981) as monoclinic (PDF 2-1012), this indexing is suspect because of the large number of $k \neq 3n$ indices required. We consider that the trigonal form of greenalite is dominant in this sample and that impurities account for the large number of weak lines present that are not observed on any of our patterns. In quartz-free samples (Fig. 1b), or in samples where the quartz impurity is coarse grained and gives a spotty powder pattern (Fig. 1a), the 2.486 \AA line can be used as an indicator of the presence of the monoclinic component. In this way it has been possible to detect the monoclinic component in all samples examined in this study. Where the sample consists of a single small granule, monochromatic Fe X-radiation was found to be necessary to detect very small concentrations of the monoclinic component.

Electron-diffraction study

The three purest greenalite samples, from Cartagena (Spain), the Sokoman Iron Formation (Labrador) and the Bluebell mine (British Columbia), were selected for electron microscopy and electron diffraction. The samples were prepared in two ways. Samples that were prepared by ion thinning revealed that the individual granules are composed of an anastomosing mass of intergrown laths. Individual laths within the granules could not be isolated in these composite specimens, even with the smallest apertures available to us on the JEOL 100B electron microscope. Isolation could be achieved by abrading a greenalite-rich rock with an iron file and dispersing the particles onto a glass slide coated with a monolayer soap film. The particles were then carbon-coated, floated off the slide and mounted on a copper TEM mesh for study.

All electron-diffraction photographs of the $hk0$ network of greenalite show only a single set of orthohexagonal $k = 3n$ spots, but with each spot surrounded by a hexagonal array of satellite spectra. Characteristically, the hexagon is incomplete, with the satellites closest to the direct beam being weak or absent (Fig. 2). Only a few higher-order satellites are observed.

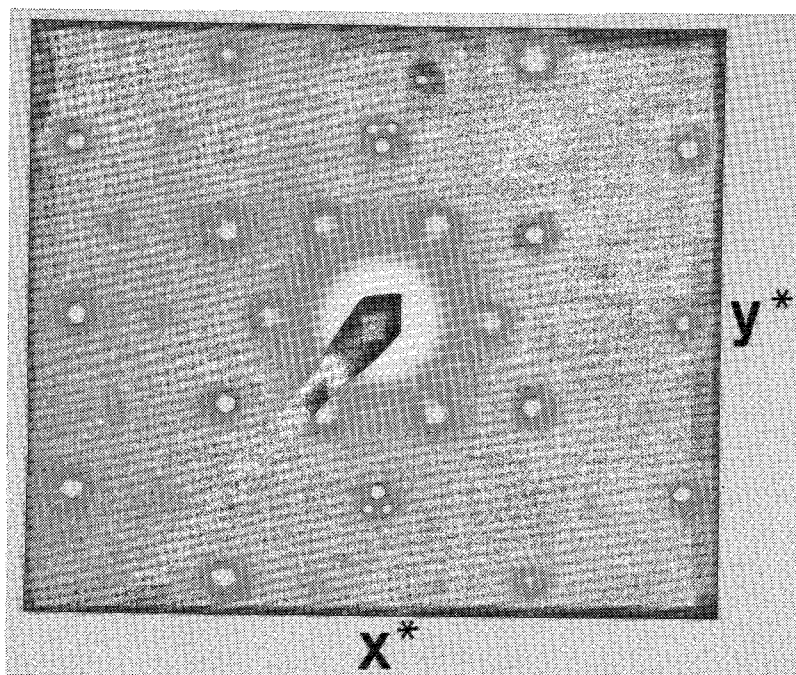


FIG. 2. Electron-diffraction photograph of the $hk0$ net of greenalite from Cartagena, Spain.

The separation of a satellite from its central spot indicates a regular modulation of the sub-cell structure that measures 23.3 to 21.3 Å in the three specimens. The satellites always are aligned along the three pseudohexagonal Y^* axes (normal to the three pseudohexagonal X axes). Electron-diffraction photographs of several berthierine flakes for comparison purposes were found to give only $hk0$ networks without satellites. This emphasizes the essentially different nature of the structures and perhaps of the relationship between the two phases present in berthierine and greenalite.

On the $hk0$ electron-diffraction photographs of greenalite, all $k = 3n$ reflections are sharp. In Figure 2 the intensity is zero right at the $k \neq 3n$ lattice points, and the diffuse intensity extends radially away from the lattice points in both the positive and negative directions along one of the Y^* axes. In the especially well-crystallized greenalite from the Sokoman Iron Formation in Quebec, the outer diffuse concentrations of intensity that are single in Figure 2 are split sideways along X^* into two distinct lobes similar to those shown in Figure 6c for caryopilite.

A few nets other than that for $hk0$ were observed on the electron-diffraction photographs, although in all cases multiple "grains" were

involved. Several $h0l$ orientations were obtained, each showing oriented intergrowths of the trigonal and monoclinic phases (Fig. 3). The $20l$ trigonal and monoclinic spots are connected by diffuse streaks indicating coherency of intergrowth. Only a few monoclinic spots are seen because the $h0l$ reciprocal nets for the two phases are not coplanar. The orientation of the two phases deduced from these photographs is exactly that found in the single-crystal X-ray study of the Bluebell mine greenalite. The β angle of the monoclinic phase was measured as 104.5 to 105.5° on different photographs.

Electron microscopy

One possible interpretation of satellites in which two phases are known to be present is that the satellites are due to multiple diffraction resulting from a coherent intergrowth of one phase imbedded in and slightly rotated relative to a matrix of a second phase [e.g., Mg_3Si platelets in a host crystal of metallic Al, discussed by Hirsch *et al.* (1965, p. 151-152)]. This was our first interpretation, expressed only in abstract form (Guggenheim *et al.* 1977). This interpretation was disproved by subsequent optical imaging.

For all the greenalite specimens studied by electron diffraction, introduction of a single

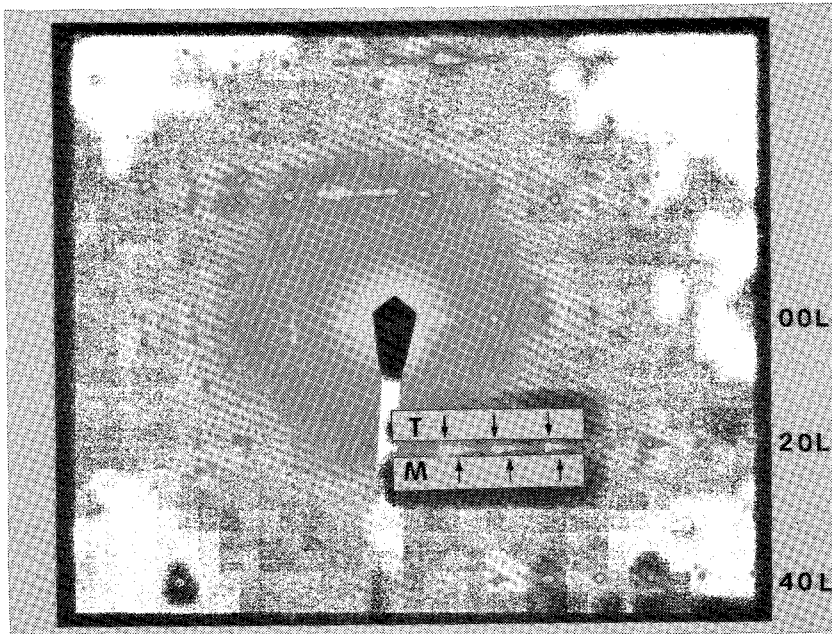


FIG. 3. Electron-diffraction photograph of the $h0l$ net of greenalite from Cartagena, Spain. Reflections from both the trigonal and monoclinic phases are visible along the $20l$ row lines.

200 reflection plus its satellites into the microscope objective produced three sets of inter-

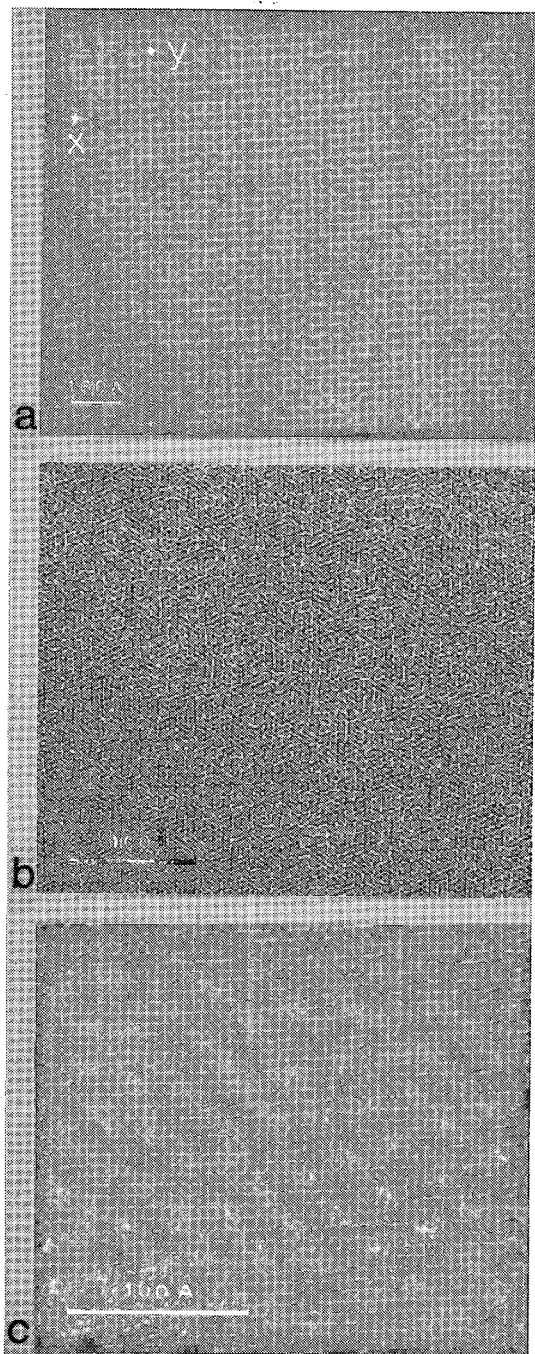


FIG. 4. Lattice fringe images of the (001) plane of greenalite from Cartagena, Spain. a) Showing the 23 Å domains. b) and c) Showing irregularity in the 4.6 Å 020 and 110 lattice fringes.

secting lattice fringes that are normal to the three pseudohexagonal Y^* axes. Although slightly irregular in shape and direction, the fringes have average periodicities between 21 and 23 Å. Within the accuracy of measurement (± 1.0 Å), the fringe separations are in agreement with the separation of a satellite from its central spot on the electron-diffraction pattern of each specimen. It can be concluded that the satellites are due to a regular modulation of the subcell structure along the three pseudohexagonal Y axes. The satellites are irrational in that the indicated modulations (S) are not integral multiples of the conventional subcell dimensions ($2.4b_c$ to $2.2b_c$ for these specimens). If $S = 2.33b_c$, as in the Sokoman greenalite, a superlattice of $a = 27.9$ Å = $5a_c$, $b = 45.2$ Å = $4.67b_c$ can be described in the X - Y plane (ignoring the extinguished $k \neq 3n$ reciprocal lattice points).

The greenalite from Cartagena (Spain) was examined also with a JEOL 200CX electron microscope in the laboratory of Professor B. G. Hyde in Canberra. In addition to dark field images produced using a single 200 reflection plus its satellites, bright field images were obtained with the objective opened to include all reflections out to 200 and equivalent indices plus their satellites. The increased resolution with this instrument showed that the 23.3 Å fringes consist of domains containing about 12 tetrahedral rings (Fig. 4b, c). The domains show considerable variation in size and shape, and the interdomain region is poorly defined. It is evident that there is considerable irregularity and defect associated with the 23.3 Å superstructure, even in this well-crystallized specimen. In edge views parallel to (001), the individual sheets appear crinkled in some areas (Fig. 5a), somewhat similar to those of antigorite. Because the superstructure extends in three directions within (001), the crinkled nature of Figure 5a should not be interpreted as a single alternating antigorite-like wave. It is possible that the domains are saucer-shaped, owing to sheet misfit, and that some adjacent domains are inverted relative to one another.

MANGANESE-RICH SAMPLES

The Mn^{2+} -analogue of greenalite is caryopilite, sometimes called bementite in the older literature (Kato 1963). The structure of caryopilite has been determined by Shirozu & Hirowatari (1955) to be a 1M polytype with a serpentine-like structure. However, we find

that X-ray powder patterns of four specimens (Fig. 1, Tables 3, 4) in all cases show a small amount of a trigonal phase in addition to the dominant monoclinic host. No $k \neq 3n$ reflections are present for either phase, and the precise polytypes cannot be established.

Electron-microprobe analyses of the caryopilite samples are similar to those of greenalite in that there is an apparent excess of Si and an apparent octahedral deficiency upon calculation of the structural formula on the basis of seven oxygens (Table 5). The Si ranges from 2.08 to 2.20 atoms per formula unit, quite similar to the Si values for greenalite. The octahedral deficiencies range from 0.23 to 0.45 atoms, being somewhat larger than the greenalite values (0.15 to 0.27). The deficiencies also are greater than those of

TABLE 4. MANGANESE-RICH SAMPLES STUDIED

Locality and Occurrence	Donor
1. Caryopilite. Hurricane Claim, Olympic Peninsula, Wash., U.S.A. Sorem spec. #S-60-14-16. Tertiary age granules in sediments.	R. K. Sorem
2. Caryopilite. Olympic Mountains, Wash., U.S.A. AMNH spec. #19258 labeled "bementite".	AMNH
3. Caryopilite. Fallota, Grisons, Switzerland AMNH spec. #32380 labeled "bementite".	AMNH
4. Manganoan lizardite. Harstigen mine, Persberg district of Värmland, Sweden. K. Eldjarn coll. #466b, fibrous veinlets labeled "caryopilite". Fissure veins in metamorphosed Precambrian limestones.	D. H. Garske
5. Caryopilite. Ichinomata mine, Kumamoto Prefecture, Kyushu, Japan.	H. Shirozu
6. "Tosalite". Matsuo mine, Kochi Prefecture, Honshu, Japan. In sedimentary strata of Paleozoic age.	H. Shirozu

TABLE 5. ELECTRON-PROBE ANALYSES OF Mn-RICH SAMPLES

	Caryopilite, #S-60-14-16				Caryopilite, AMNH #19258				Caryopilite, AMNH #32380			
	1	2	3	4	1	2	3	4	1	2	3	4
Si	35.4%	2.103	1.950	2.000	35.4%	2.077	1.853	2.000	37.9%	2.176	1.953	2.000
Al	0.78	.054	.050	.052	2.38	.165	.147	.159	0.78	.053	.047	.049
Fe*	0.72	.035	.033	.034	0.95	.047	.042	.045	0.94	.045	.041	.042
Mn	52.1	2.626	2.434	2.497	49.2	2.445	2.182	2.354	47.0	2.286	2.051	2.101
Mg	0.58	.051	.048	.049	1.23	.108	.096	.104	2.78	.238	.213	.218
□		.234	.485	.368		.235	.680	.338		.378	.695	.590
Na	0.15				0.05				0.00			
K	0.02				0.03				0.00			
Ca	0.00				0.16				0.27			
Σ	89.75				89.40				89.67			
	Caryopilite, Ichinomata mine				Mn-lizardite, Harstigen mine				"Tosalite", #1977-4			
	1	2	3	4	1	2	3	4	1	2	3	4
Si	38.9%	2.200	1.917	2.000	45.1%	2.168	1.974	2.000	32.8%	1.935	1.802	2.000
Al	1.44	.096	.083	.087	0.51	.029	.026	.027	3.05	.212	.198	.220
Fe*	0.48	.023	.020	.021	0.65	.026	.024	.024	43.6	2.153	2.005	2.226
Mn	47.0	2.252	1.961	2.047	16.25	.662	.602	.611	5.87	.294	.274	.304
Mg	2.15	.181	.158	.165	27.0	1.932	1.759	1.782	4.16	.366	.341	.379
□		.448	.861	.680		.351	.615	.556		.040	.380	(+.129)
Na	0.00				0.00				0.00			
K	0.12				0.00				0.01			
Ca	0.00				0.13				0.00			
Σ	90.09				89.64				89.49			
	"Tosalite", #1977-6				"Tosalite", #1977-12				"Tosalite", #1977-8			
	1	2	3	4	1	2	3	4	1	2	3	4
Si	32.9%	1.896	1.663	2.000	34.7%	1.985	1.705	2.000	34.6%	1.976	1.711	2.000
Al	5.65	.384	.337	.406	5.09	.343	.295	.346	4.96	.334	.289	.338
Fe*	40.6	1.957	1.717	2.065	38.5	1.842	1.582	1.856	39.7	1.896	1.642	1.919
Mn	6.54	.319	.280	.337	7.97	.386	.332	.389	8.52	.412	.356	.417
Mg	4.14	.356	.312	.375	3.37	.287	.247	.290	2.82	.240	.207	.242
□		.088	.691	(+.183)		.157	.839	.119		.142	.795	.084
Na	0.00				0.22				0.05			
K	0.00				0.08				0.02			
Ca	0.00				0.22				0.16			
Σ	89.83				90.15				90.83			

* All Fe reported as FeO 1. Weight percentage of oxides 2. Atoms on basis of 7.0 oxygens
3. Atoms on basis of 2.0 Si+Al tetrahedral cations 4. Atoms on basis of 2.0 Si tetrahedral cations

greenalite after tetrahedral site allocations of 2.0 Si and 2.0 Si+Al atoms (Table 5). No information is available on the valence state of Mn in these samples. The caryopilite samples are less pure than the greenalite samples, and electron diffraction has revealed the presence

of other Mn-rich minerals. Thus, the analyses of Table 5 may partly reflect these impurities. For example, most of the Al and all of the K in the analysis of the Ichinomata mine (Japan) specimen are believed to be present in a bannisterite-like phase.

Kato (1963) has shown that hexagonal arrays of satellites occur around the $k = 3n$ spots on electron-diffraction photographs of

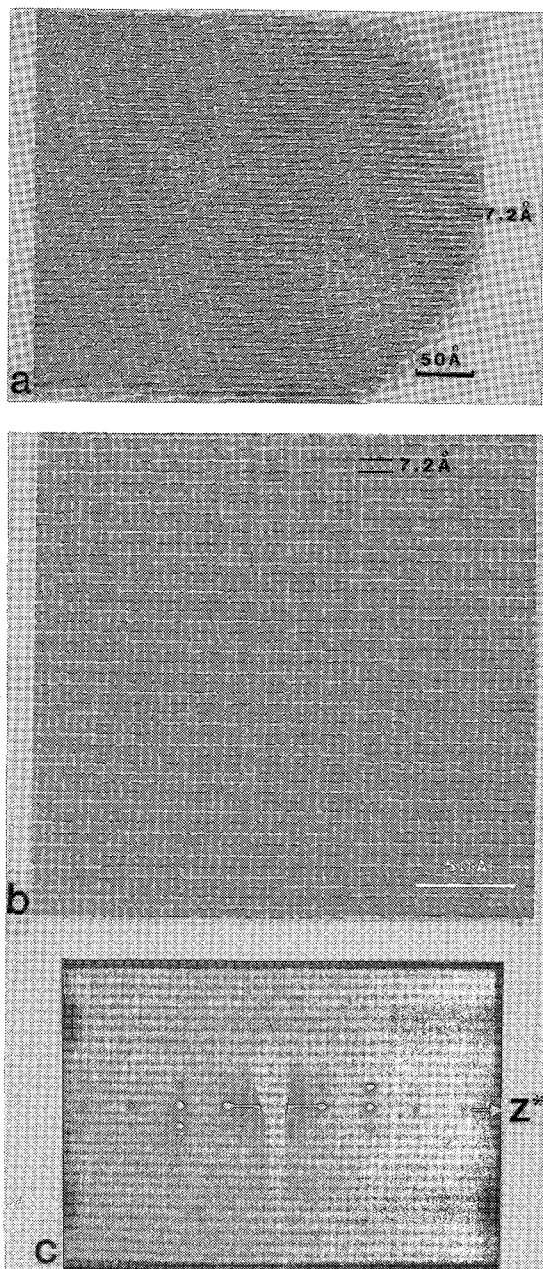


FIG. 5. Lattice fringe images of the 7 Å layers approximately parallel to (001). a) Greenalite from Cartagena, Spain. b) Caryopilite from Ichinomata, Japan. c) Electron-diffraction pattern of crystal shown in b).

caryopilite. We have confirmed this for the caryopilites from Ichinomata (Japan), Olympic Mountains (U.S.A.) and Fallota (Switzerland), as well as for a manganoan lizardite. The latter specimen from Harstigen (Sweden), although labeled "caryopilite" when received and similar in appearance to the other specimens, actually contains 27% MgO by analysis. The X-ray powder pattern differs from that of caryopilite in that the two phases present are both monoclinic but with slightly different cell dimensions.

Caryopilite $hk0$ electron-diffraction patterns show a range of detail in the 020 family of reflections, from rather diffuse blobs similar to those in greenalite (Fig. 6a) to a sharper group of three reflections (Fig. 6c). Electron-optical lattice fringes of caryopilite are similar to those of greenalite in the X - Y plane. Side views parallel to (001) (Fig. 5b) show more clearly the sinusoidal modulation of essentially continuous sheets.

When the separation of an electron-diffraction satellite from its central $k = 3n$ reflection is plotted versus $b_0 = 6d(060)$, as measured from the X-ray powder pattern for the same specimen, there is an apparent linear trend from modulations near 23 Å for greenalite to 17 Å for caryopilite (Fig. 7, Table 6). Consequently, the irrational values of the satellites change from $2.4b_0$ to $1.7b_0$. Because of the small number of intermediate compositions, an alternative interpretation of the plot in Figure 7 is that the variation is step-like, with modulations grouped near 23, 21 and 17 Å for the specimens of this study.

The amount of the monoclinic phase present also varies as a function of $d(060)$ and MnO content, although not in a linear fashion. The greenalites closest to the Fe end-member composition (specimens 1, 5, 6 and 7 in Table 1) have the smallest amounts of the monoclinic phase, which require monochromatic X-radiation for detection when individual small granules are used as samples. Greenalite 4 and 8, with 1.78 and 1.50% MnO by analysis, respectively, have slightly larger amounts of the monoclinic phase. Precise determination of the amount of the monoclinic phase present is difficult for all of these specimens because of the varying purity of the granules used. For the Bluebell mine greenalite with 8.71% MnO, the two phases are present in roughly equal amounts. For end-member caryopilites the monoclinic phase is dominant, and the trigonal phase requires monochromatic X-radiation for detection when using small granules.

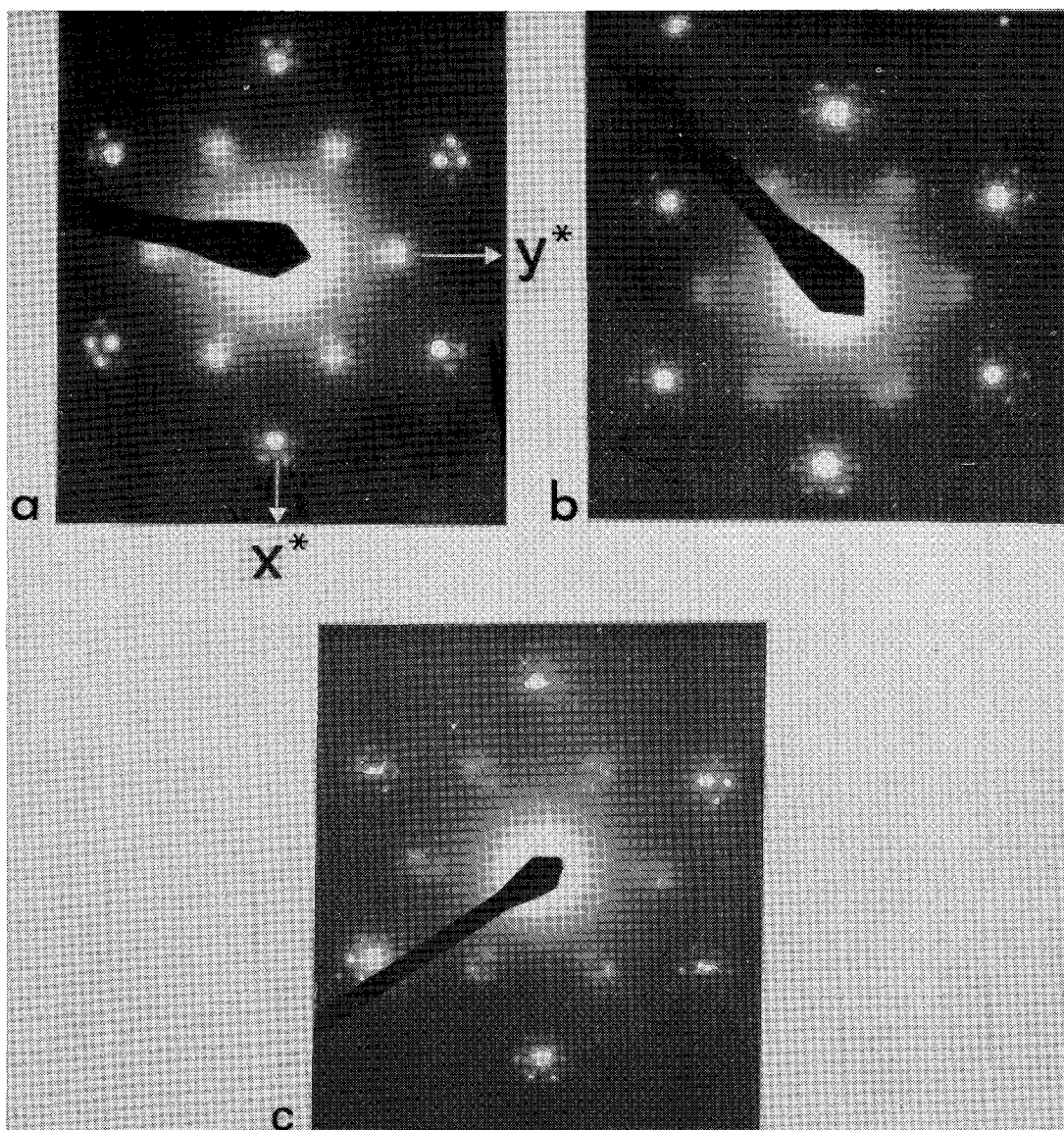


FIG. 6. Electron-diffraction patterns of diffuse intensity associated with vacant $k \neq 3n$ positions for a) Cartagena greenalite, b) Ichinomata caryopilite and c) Fallota (Switzerland) caryopilite.

The combination of X-ray and electron-diffraction results for these specimens shows that the same modulation effect and the same inter-growth of phases observed for greenalite occur at the Mn end of the series as well. The two phases in caryopilite are in the reverse order of abundance relative to greenalite; the monoclinic phase is dominant. The similarities to greenalite clearly indicate caryopilite to be its Mn-analogue.

Peacor & Essene (1980) have argued that caryopilite is a member of the friedelite group of minerals, rather than being a true serpentine. They based their conclusion on the similarity of the powder patterns for caryopilite and friedelite plus their electron-microprobe analyses for caryopilite. The latter gave a ratio of octahedral cation to silicon close to 8:6, as in friedelite, rather than the 9:6 ratio expected for a serpentine-like structure. But we note that the

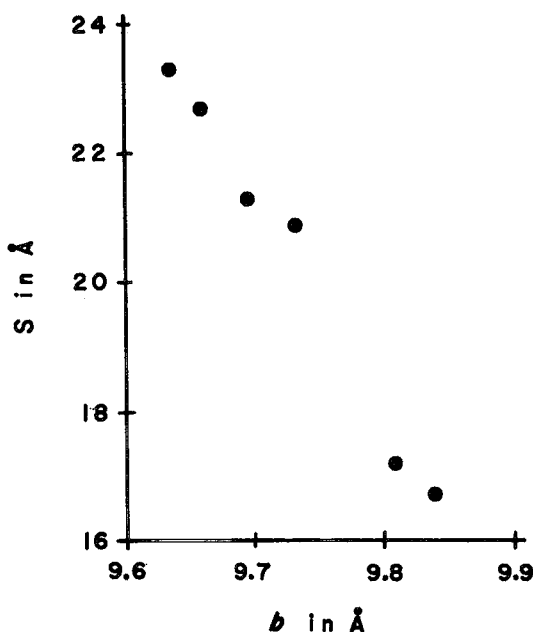


FIG. 7. Plot of satellite separation S versus b parameter.

lateral cell-dimensions of friedelite for a C -centred cell (a 5.81, b 10.05 Å) are appreciably larger than those of our most Mn-rich caryopillite (a 5.69, b 9.86 Å), and that electron-diffraction photos of friedelite do not show satellites to the $k = 3n$ reflections. Thus, the detailed structures of caryopillite and friedelite must be different. It may be, as suggested by Peacor (pers. comm. 1981), that caryopillite represents a structure transitional between that of a true serpentine and friedelite.

Yoshimura (1967) has described tosalite from the Tosa mine, Japan, as an intermediate member of the greenalite-caryopillite series (MnO 34.78, FeO 11.97, Fe₂O₃ 8.49%). We have examined a less Mn-rich sample labeled "tosaitite" from the Matsuo mine, Japan. X-ray powder patterns show that the proportions of

the monoclinic and trigonal phases are variable from place to place in our hand sample, but $d(060)$ is always close to that of greenalite rather than of caryopillite. Electron-microprobe analyses (Table 5) of four of the same granules for which X-ray patterns were taken show only 5.87 to 8.52% MnO, so that these granules from the Matsuo mine probably should be classified as manganoan greenalites.

More Al₂O₃ is present in these Matsuo greenalite granules (3.05 to 5.65%) than in the other greenalites; we interpret Al to be in both tetrahedral and octahedral positions, as given by the structural formula allocations in Table 5. For example, two analyses yield more than 3.0 total octahedral cations on the basis of 2.0 tetrahedral Si atoms per formula unit; the other two analyses yield unreasonably low octahedral cation totals (2.16 and 2.20) on the basis of 2.0 tetrahedral Si+Al cations (*i.e.*, all Al in tetrahedral coordination). It is unlikely that a large amount of Al₂O₃ can be incorporated in a true greenalite structure, because substitution of Al in either tetrahedral or octahedral positions would tend to alleviate the lateral misfit of sheets and to produce the berthierine structure instead. We have verified by X-ray powder patterns that the "Al-greenalite" from the Ruth shale of the Sokoman Iron Formation, described by Klein & Fink (1976) as having up to 12% Al₂O₃, is berthierine rather than greenalite.

The Matsuo greenalite analyses provide further evidence for variation in concentration of the monoclinic phase in proportion to the amount of MnO present. Particle 1977-4, with the monoclinic phase judged to be least abundant from the powder pattern, has the least MnO by analysis (5.87%). Particle 1977-6 has slightly more MnO (6.54%), and the two phases are approximately equal in abundance. The two particles with the monoclinic phase most abundant (1977-8-12) have the most MnO by analysis (7.97 and 8.52%). The distribution of other octahedral cations between the two phases may be also of importance, possibly leading to the concentration of smaller cations in the trigonal phase. It is noted, for example, that about equal proportions of the two phases are obtained at a higher MnO concentration (8.71%) for the Al-poor Bluebell mine greenalite than for the more Al-rich Matsuo greenalite 1977-6 (6.54%).

TABLE 6. SATELLITE SEPARATIONS

Sample	$S =$ separation satellite from main spot	$b = 6 \times d(060)$	S/b ratio
greenalite Cartagena, Spain	23.3A	9.636Å	2.42
greenalite Sokoman Iron Fa., Labrador	22.7	9.660	2.35
greenalite Bluebell mine, B.C.	21.3	9.696	2.20
Mn-lizardite Sweden	20.9	9.732	2.14
caryopillite Ichinomata, Japan	16.7	9.840	1.70
caryopillite Fallota, Switzerland	17.2	9.810	1.75

SUMMARY OF DATA FOR GREENALITE-CARYOPIILLITE

The experimental data that must be ex-

plained for a complete understanding of the structural nature of greenalite and caryopilite are summarized below. Because our interpretation is incomplete, it is important that fact and interpretation be clearly separated. (1) Electron-microprobe analyses of greenalite and caryopilite consistently show an excess of Si and a deficiency of total octahedral cations upon allocation on the basis of seven oxygens for a serpentine-type structure. (2) Both a trigonal and a monoclinic phase are present in all greenalite, caryopilite and intermediate composition specimens studied. Whenever the relative orientations could be determined, the two phases were found to be in a fixed, coherent intergrowth, with one phase either rotated by 180° (or $\pm 60^\circ$) relative to the other or inverted without rotation. Rotation is equivalent to occupation of a different set of octahedral positions. (3) On $hk0$ electron-diffraction photographs, the $k = 3n$ reflections are sharp and are surrounded by incomplete hexagons of satellites directed along the three pseudo-hexagonal Y^* axes. Higher-order satellites occur infrequently. The satellite spacings indicate a regular but irrational modulation of the subcell structure, varying from $23 \text{ \AA} = 2.4b_0$ in greenalite to $17 \text{ \AA} = 1.7b_0$ in caryopilite. (4) On $hk0$ electron-diffraction photographs, the $k \neq 3n$ indices have zero intensity at the lattice points. Outside these lattice points, there is a distribution of diffuse intensity that varies from two to three ill-defined blobs to three sharper superlattice spots. (5) Electron micrographs show three sets of intersecting fringes normal to the three pseudo-hexagonal Y^* axes, which can be resolved into domains consisting of a small number of tetrahedral sixfold rings. The domain boundaries are poorly resolved, and there is considerable defect nature in the size, shape and lateral disposition of the domains. Lattice fringes normal to the (001) layers have a crinkled to sinusoidal appearance in places.

INTERPRETATION

We have attempted to integrate the experimental observations into a single structural model. We make the basic assumption that the observed structural modulations are due to the inherent lateral misfit between a larger Fe, Mn-rich octahedral sheet and a smaller Si-rich tetrahedral sheet. The modulations of 23 to 17 \AA found for greenalite and caryopilite are comparable to values of (1) 21.6 \AA found for the extent of articulation between misfit sheets in a single wave of antigorite by Kunze (1956)

and of (2) 21.6 to 22.0 \AA found between inverted islands in the structure of stilpnomelanes of different composition by Eggleton (1972). In both cases, rational superlattice reflections rather than irrational satellites are present, and the lateral misfit of sheets is accommodated by some regular pattern of tetrahedral inversion and relinkage. The significance of these superlattice values is that they give a measure of the lateral extent to which the misfit sheets can maintain linkage for these compositions before the strain must be relieved by some form of structural modulation.

The [001] images and diffraction patterns imply a structure for greenalite in which one extra tetrahedron is inserted into the tetrahedral sheet approximately every eight tetrahedra (Fig. 8). This enlarges the tetrahedral sheet sufficiently for it to fit with an octahedral sheet which, if unconstrained, would exceed the dimensions of the tetrahedral sheet by a factor of $16/15$. Where the octahedra articulate with the apical oxygens of the tetrahedral "islands" of six-member rings, the octahedral sheet contracts in the X - Y plane, probably by curving. Around the edges of the islands, the three- and four-member rings are postulated as inverted so that they coordinate with the octahedral sheet of the adjacent layer. It is also possible that entire islands are inverted in a similar fashion. The micrographs show that the real structure is much less regular than this model. On average, the islands are four rings in diameter, but individual islands may be smaller or may not be equidimensional. Optical simulation of the $hk0$ diffraction pattern using this regular model reproduces the satellites to the $k = 3n$ reflections quite well, but naturally has many other sharp superlattice reflections. A model in which each island in the diffraction mask (Fig. 9b) is randomly displaced by one octahedral anion vector from its ideal position allows simulation of the coordination of each silicon pair to different pairs of apical oxygens from among the anions of the octahedral sheet on a random basis. The resulting optical diffraction pattern (Fig. 9a) introduces diffuse $k \neq 3n$ reflections while still leaving the $k = 3n$ satellites sharp. This simulation compares reasonably well with the greenalite electron-diffraction patterns, differing primarily in the details of the $k \neq 3n$ reflections.

Lattice fringes of greenalite viewed parallel to (001) show, at least in some areas, a wavy structure (Fig. 5a). This suggests that the structure resembles a stack of saucers, in which the convex upward octahedral saucers fit as caps over the tetrahedral islands of Figure 8.

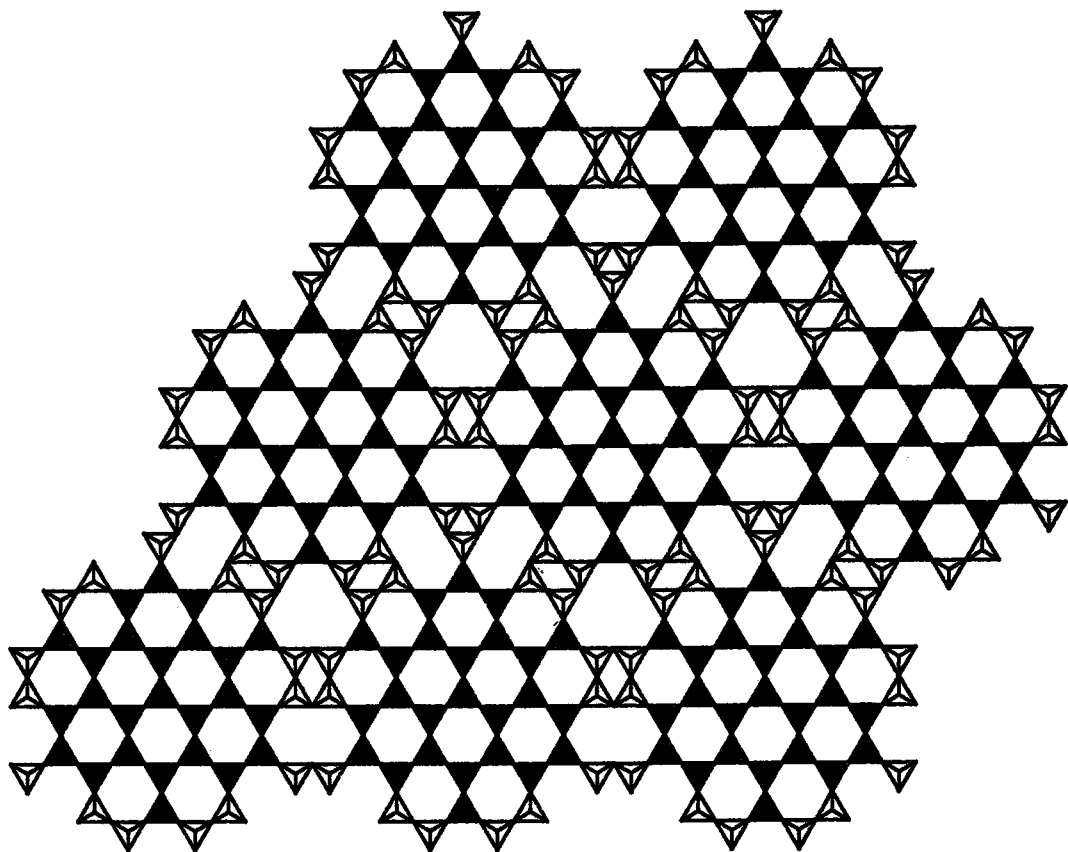


FIG. 8. Idealized tetrahedral sheet for greenalite.

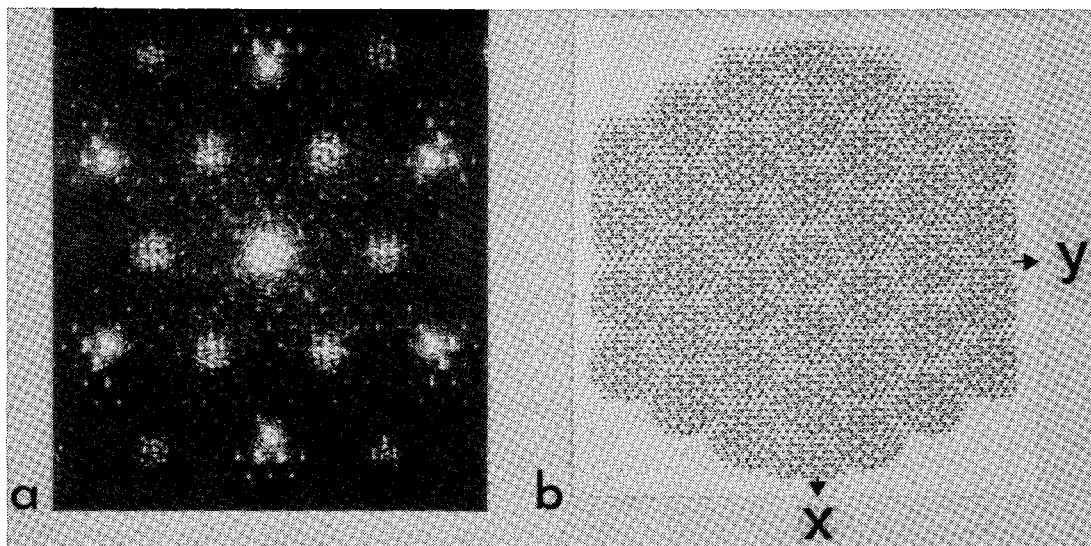


FIG. 9. a) Optical diffraction pattern of the mask shown in b). b) Diffraction mask for regular octahedra and a tetrahedral sheet as in Figure 8, but with tetrahedral islands coordinating randomly to octahedral anion positions.

The images from caryopilite allow this model to be extended and modified. Caryopilite from Ichinomata (Japan) has a smaller modulation, indicated by the $k = 3n$ satellites, than in greenalite, consistent with a model tetrahedral sheet having islands about three hexagonal rings in diameter instead of four. Images parallel to the subcell [100] direction show reasonable continuity along Z of the superlattice modulation (Fig. 5b). The distributions of diffuse intensity outside the positions of the extinguished $k \neq 3n$ reflections on $hk0$ electron-diffraction patterns of this specimen are more widely separated (Fig. 6b) than in most greenalites studied. In caryopilite from Fallota (Switzerland), three sharper satellites or superlattice reflections are found in these positions (Fig. 6c). This indicates a second modulation system that is more regularly developed in some specimens than in others.

Our interpretation of the two apparently independent modulation systems involving $k = 3n$ and $k \neq 3n$ reflections is based on a consideration of the Fourier transform of the substructure. X-ray and electron scattering from layer silicates is dominated by the trigonal subcell of octahedral cations that repeat at intervals of about $3.2 \text{ \AA} = b_c/3$ of the conventional cell. Consequently, there is strong scattering centred on reciprocal lattice points for which $k = 3n$. The octahedral anions have the same subcell and contribute to these same reflections. The tetrahedral cations, although falling on the same subcell, are missing from one out of three lattice points; this, together with the contributions from the basal oxygens, introduces scattering between the subcell reflections at the so-called $k \neq 3n$ positions.

Strong satellite reflections around $k = 3n$ subcell reflections result from perturbations to the subcell that are responsible for the strong subcell reflections. Thus, for example, a regular distortion of the octahedral sheet cannot produce satellites at the $k \neq 3n$ positions, because the octahedral sheet transform has low intensity in this region. Similarly, modulations of the tetrahedral sheet cannot cause satellites to $k = 3n$ reflections alone, because the tetrahedral sheet also scatters significantly at $k \neq 3n$ positions. We therefore interpret the hexagonal pattern of satellite reflections found around the $k = 3n$ reflections as resulting from a periodic distortion of the octahedral sheet. In caryopilite from Fallota (Switzerland), the triangle of reflections found about the position where 020 would be in a normal layer silicate (Fig. 6c) results from a periodic variation in the tetra-

hedral sheet. The lack of perfect regularity in both octahedral and tetrahedral distortions prevents the development of a larger superlattice that would enclose rational numbers of octahedral- and tetrahedral-distortion supercells along both X and Y . As a result, only first-order satellite reflections to the sublattice points are observed.

We suggest that the distortion of the octahedral sheet in both greenalite and caryopilite is caused by a combination of the periodic doming of the octahedral saucers associated with the tetrahedral islands plus rows of octahedral vacancies around each saucer, where inversion of rings probably takes place and articulation of the two sheets is difficult. Because observed $k = 3n$ reflections are sharp, the scattering from the octahedral sheet must be in-phase and relaxation effects in the vacant boundary octahedra may help achieve this coherency. Optical simulation of the observed diffraction patterns has been achieved by a periodic contraction of the octahedral sheet where it articulates to the tetrahedra, and a release to its unconstrained dimension where the tetrahedra invert. But any model in which the mean octahedral size is greater than the mode should give rise to a similar octahedral superlattice. The lower intensities of the satellites on the origin side of the $k = 3n$ reflections are due to the incommensurate nature of the modulation in which the supercell dimension is slightly greater than that of $3n$ subcells, as duplicated in the optical simulation pattern (Fig. 9a).

No $k \neq 3n$ reflections are observed on any of the diffraction patterns, and this is taken into account in our model by the introduction of four-member rings at the tetrahedral island edges, which cause adjacent islands to be out-of-phase by $a/2$. At the same time, the four-member rings provide the extra tetrahedra necessary to continue linkage with the octahedral sheet (Fig. 8). Our model thus explains the observed nonstoichiometry of greenalite and caryopilite relative to true serpentine as due both to the introduction of extra tetrahedra and also to the omission of octahedral cations. In greenalite some of these vacancies are associated with Fe^{3+} ions. It is also possible that some octahedral OH groups are omitted at the inversion regions of the island boundaries, as is the case with antigorite. Our data do not allow quantification of nonstoichiometry. The diffuse blobs near the $k \neq 3n$ positions in diffraction photos of greenalite indicate that the superlattice involving distortions in the tetrahedral sheet is

incompletely developed in greenalite, in contrast with the sharper superlattice reflections in Fal-lota caryopilite. Further imaging and modeling work is in progress for the Mn-rich specimens.

The imaging study has not provided any information as to the nature or origin of the trigonal and monoclinic phases known to be present in all samples. One possible explanation is that unmixing has segregated the Fe-rich and Mn-rich compositions in a fixed, coherent structural relationship. In particular, one might expect misfit cations to locate preferentially in the inter-island regions, where a different mode of layer stacking might be initiated. The fact that greenalite specimens 1, 5 and 6 (Table 1) have very small amounts of MnO by analysis (0.15, 0.18 and 0.06%, respectively, from Table 2), yet detectable amounts of the monoclinic phase, is evidence against this strictly compositional interpretation. The presence of two phases in all samples suggests that the two phases are related in some manner to the structural modulation, and probably are essential to the stability of the greenalite-caryopilite structural system. Proof of the latter interpretation would require that two phases be demonstrated to be present in chemically pure synthetic greenalite and caryopilite. The X-ray powder pattern of synthetic greenalite published by Jasmund *et al.* (1976) is inconclusive on this point. There are two lines recorded at $d = 2.495$ and 2.073 Å (intensities not listed) that are close to the two strongest lines of the monoclinic phase, but it is possible that these are due to the presence of a small amount of a tubular form of greenalite.

MINNESOTAITE

Because of the linkage of greenalite with minnesotaite in the structural model of Floran & Papike (1975), we have taken a preliminary look at the diffraction patterns of minnesotaite. Although Gruner (1944) suggested that minnesotaite is the ferrous analogue of talc, X-ray powder patterns of talc and minnesotaite are only superficially similar. We have been unable to index the powder pattern of minnesotaite on the basis of either the $1Tc$ or $2M$ talc structures.

X-ray-precession and electron-diffraction photographs of minnesotaite from the Cuyuna district of Minnesota are completely different from those of greenalite and caryopilite. In addition to the normal subcell reflections, there are rational superlattice reflections indicating

that the structure must be much more complex than that of a normal phyllosilicate. This is to be expected from the lateral misfit inherent in a Si-rich tetrahedral sheet and an Fe-rich octahedral sheet. We conclude that the structure of minnesotaite is not related to that of greenalite or caryopilite; as a result, we will report our results for minnesotaite in a separate communication.

ACKNOWLEDGEMENTS

This study was supported by the National Science Foundation (grants EAR 76-6620, EAR 78-05394 and EAR 80-18222), by the Petroleum Research Fund, administered by the American Chemical Society (grant 8425-AC2), and by a University of Illinois-Chicago Faculty Summer Fellowship. Samples were kindly provided by A.M. Arribas, R.J. Floran, D.H. Garske, A.M. Goodwin, G.A. Gross, C. Klein, L. Moyd, J.J. Papike, H. Shirozu, R.K. Sorem, S.A. Tyler, B. Young, I.S. Zajac and the American Museum of Natural History. We are indebted to W.A. Dollase for the Mössbauer analysis and to Cynthia S. Anderson, J.T. Cheney, E.D. Glover, D.J. Henry and Karen L. Kimball for the microprobe analysis of samples. We thank Professor B.G. Hyde of the Australian National University Research School of Chemistry for use of his electron-microscopy and diffraction facilities. Funds for computing purposes were provided by the University of Illinois-Chicago Computer Center. The manuscript has been improved by the constructive review of D.R. Peacor.

REFERENCES

- ALBEE, A.L. & RAY, L. (1970): Correction factors for electron probe microanalysis of silicates, oxides, carbonates, phosphates, and sulfates. *Anal. Chem.* **42**, 1408-1414.
- BAILEY, S.W. (1969): Polytypism of trioctahedral 1:1 layer silicates. *Clays Clay Minerals* **17**, 355-371.
- BATES, T.F. (1959): Morphology and crystal chemistry of 1:1 layer lattice silicates. *Amer. Mineral.* **44**, 78-114.
- , SAND, L.B. & MINK, J.F. (1950): Tubular crystals of chrysotile asbestos. *Science* **111**, 512-513.
- BAYLISS, P. (1981): Unit cell data of serpentine group minerals. *Mineral. Mag.* **44**, 153-156.

- BENCE, A.E. & ALBEE, A.L. (1968): Empirical correction factors for the electron microanalysis of silicates and oxides. *J. Geol.* 76, 382-403.
- BRINDLEY, G.W. (1951): The crystal structure of some chamosite minerals. *Mineral. Mag.* 29, 502-525.
- EGGLETON, R.A. (1972): The crystal structure of stilpnomelane. II. The full cell. *Mineral. Mag.* 38, 693-711.
- & BAILEY, S.W. (1967): Structural aspects of dioctahedral chlorite. *Amer. Mineral.* 52, 673-689.
- FAUST, G.T., FAHEY, J.J., MASON, B. & DWORNIK, E.J. (1969): Pecoraite, $\text{Ni}_6\text{Si}_4\text{O}_{10}(\text{OH})_8$, nickel analog of clinochrysoilite, formed in the Wolf Creek meteorite. *Science* 165, 59-60.
- FLORAN, R.J. & PAPIKE, J.J. (1975): Petrology of the low-grade rocks of the Gunflint Iron-Formation, Ontario-Minnesota. *Geol. Soc. Amer. Bull.* 86, 1169-1190.
- GRUNER, J.W. (1936): The structure and chemical composition of greenalite. *Amer. Mineral.* 21, 449-455.
- (1944): The composition and structure of minnesotaite, a common iron silicate in iron formations. *Amer. Mineral.* 29, 363-372.
- GUGGENHEIM, S., WILKES, P. & BAILEY, S.W. (1977): X-ray and electron diffraction study of greenalite and minnesotaite. *Trans. Amer. Geophys. Union (EOS)* 58, 525 (abstr.).
- HIRSCH, P.B., HOWIE, A., NICHOLSON, R.B., PASHLEY, D.W. & WHELAN, M.J. (1965): *Electron Microscopy of Thin Crystals*. Butterworths, London.
- JAGODZINSKI, H. & KUNZE, G. (1954): Die Röllchenstruktur des Chrysoitils. I. Allgemeine Beugungstheorie und Kleinwinkelstreuung. *Neues Jahrb. Mineral. Monatsh.*, 95-108.
- JASMUND, K. & SYLLA, H.M. (1970): Synthese von Eisenchrysotil. *Naturwiss.* 57, 494-495.
- , ——— & FREUND, F. (1976): Solid solution in synthetic serpentine phases. *Proc. Int. Clay Conf. (Mexico City)*, 267-274.
- KATO, T. (1963): New data on the so-called bementite. *J. Mineral Soc. Japan* 6, 93-103 (in Jap.).
- KLEIN, C., JR. & FINK, R.P. (1976): Petrology of the Sokoman Iron Formation in the Howells River area, at the western edge of the Labrador Trough. *Econ. Geol.* 71, 453-487.
- KRSTANOVIC, I. (1968): Crystal structure of single-layer lizardite. *Z. Krist.* 126, 163-169.
- KUNZE, G. (1956): Die gewellte Struktur des Antigorits. I. *Z. Krist.* 108, 82-107.
- LEITH, C.K. (1903): The Mesabi iron-bearing district of Minnesota. *U. S. Geol. Surv. Mon.* 43.
- NOLL, W. & KIRCHNER, H. (1952): Synthese des Garnierits. *Naturwiss.* 39, 233-234.
- , ——— & SYBERTZ, W. (1958): Ein weiteres Solenosilicat: Co-Chrysotil. *Naturwiss.* 45, 489.
- PEACOR, D.R. & ESSENE, E.J. (1980): Caryopilite — a member of the friedelite rather than the serpentine group. *Amer. Mineral.* 65, 335-339.
- RADOSLOVICH, E.W. (1961): Surface symmetry and cell dimensions of layer lattice silicates. *Nature* 191, 67-68.
- ROY, D.M. & ROY, R. (1954): An experimental study of the formation and properties of synthetic serpentines and related layer silicate minerals. *Amer. Mineral.* 39, 957-975.
- SHANNON, R.D. (1976): Revised effective ionic radii and systematic studies of interatomic distances in halides and chalcogenides. *Acta Cryst.* A32, 751-767.
- SHIROZU, H. & HIROWATARI, F. (1955): Bementite from the Tokuzawa mine, Fukushima prefecture. *J. Jap. Assoc. Mineral., Petrology, Econ. Geol.* 39, 241-248 (in Jap.).
- STEADMAN, R. & YOEUELL, R.F. (1958): Mineralogy and crystal structure of greenalite. *Nature* 181, 45.
- UYEDA, N., HANG, P.T. & BRINDLEY, G.W. (1973): The nature of garnierites. II. Electron-optical study. *Clays Clay Minerals* 21, 41-50.
- YOSHIMURA, T. (1967): Manganese mineralization, minerals, and ores (Part I, supplement to Manganese Ore Deposits of Japan). *Kyushu Univ. Sci. Rep., Fac. Sci.* 9, Ser. D.
- ZAJAC, I.S. (1974): The stratigraphy and mineralogy of the Sokoman Formation in the Knob Lake area, Quebec and Newfoundland. *Geol. Surv. Can. Bull.* 220.
- ZUSSMAN, J. (1954): Investigation of the crystal structure of antigorite. *Mineral. Mag.* 30, 498-512.
- ZVIAGIN, B.B. (1957): Determination of the structure of celadonite by electron diffraction. *Sov. Phys. Cryst.* 2, 388-394.